

Shadows of Kerr-Vaidya-like black holes

Hai Siong Tan

University of Pennsylvania, Perelman School of Medicine, Department of Radiation Oncology,
Philadelphia, USA

JAN 2023

Abstract

In this work, we study the shadow boundary curves of rotating time-dependent black hole solutions which have well-defined Kerr and Vaidya limits. These solutions are constructed by applying the Newman-Janis algorithm to a spherically symmetric seed metric conformal to the Vaidya solution with a mass function that is linear in Eddington-Finkelstein coordinates. Equipped with a conformal Killing vector field, this class of solution exhibits separability of null geodesics, thus allowing one to develop an analytic formula for the boundary curve of its shadow. We find a simple power law describing the dependence of the mean radius and asymmetry factor of the shadow on the accretion rate. Applicability of our model to recent Event Horizon Telescope observations of M87* and Sgr A* is also discussed.

Contents

1	Introduction	2
2	A family of rotating Vaidya-like black hole solutions	4
2.1	Conformal factors, coordinate charts and the Newman-Janis algorithm	4
2.2	Horizons in the solution parameter space	6
3	Null geodesics, photon spheres and shadow formulas	8
3.1	On null geodesics	8
3.2	Shadow formulas from photon region	9
4	Portraits of the shadow	10
4.1	Scaling laws for variation of \bar{R} and \mathcal{A} with μ	11
4.2	On the shadows of M87* and Sagittarius A* as observed by EHT	14
5	Discussion	16
A	Global geometry and matching spacetimes via junction conditions	17
B	On the reference frame of the shadow observer	19
B.1	In the limit of $a = 0$	19
B.2	Observers in the $\{v, w, \theta, \phi\}$ chart and aberration formulas	19

1 Introduction

Recent Event Horizon Telescope (EHT) observations of horizon-scale shadow images of M87* [1] and Sgr A* [2] have furnished not only a direct visual evidence of black holes, but have also led to many new constraints on various potential deviations from General Relativity. The boundary curve of the black hole shadow emerges from light rays that spiral asymptotically from the photon region demarcating the borderline between light rays that will eventually be captured by the black hole and those that escape to infinity [3].ⁱ The geometry of this boundary curve depends on the background metric which could thus be probed by EHT observations [7, 8, 9]. For example, the shadow geometry of Sgr* has been used to exclude the central object being a Reissner-Nordstrom-type naked singularity or a traversable Misner-Thorne wormhole [8].

Surrounding the black hole shadow is an emission ring of which structure is sensitive to a rich set of astrophysical phenomena, such as radiative transfer, that characterize the matter-energy accretion process. Typically, general relativistic magnetohydrodynamic (GRMHD) simulations are used to model the accretion flow processes [7, 8, 10, 11]. For the EHT experiments, they have revealed the emission ring properties to be consistent with a number of accretion models built

ⁱThis curve is termed as the ‘critical curve’ by Gralla et al. in [4] and ‘apparent boundary’ by Bardeen in [5]. See for example the review of [6] for an extensive discussion of basic ideas and history.

upon the background of a Kerr black hole [7, 8]. The spacetime metric in these simulations is assumed to be purely Kerr spacetime throughout, with the energy-momentum tensor capturing the magnetic field and average plasma properties [10, 12]. In [13, 14, 15], it was noted that the shadow size and shape is hardly influenced by the accretion details, and thus serves as a pristine signature of spacetime geometry. An implicit assumption is that the backreaction of the GRMHD energy-momentum tensor on the metric has a negligible influence on the shadow and could thus be ignored in deriving its geometry.

In this paper, we study the shadow boundary curves of a class of rotating time-dependent black hole solutions of which metric is a deformation of the Kerr solution described by a small dimensionless parameter μ . In the limit of vanishing spin, our spacetime reduces to a well-known model of spherically accreting black hole - the Vaidya spacetime with a mass function μv , with v being an ingoing Eddington-Finkelstein coordinate and μ being the mass accretion rate constant in natural units. The latter solution was studied most recently in [16] where the authors derived and examined its shadow characteristics analytically. Most crucially, an analytic treatment of the shadow was possible by virtue of the existence of a Carter constant leading to separability of its null geodesic equations. This is related to a conformal Killing symmetry associated with the linear mass function, and hence its choice, for it enables the authors of [16] to derive explicit formulas for the radius of the photon sphere and the shadow angular diameter. One main motivation of our work here is to seek a rotating generalization of the analytic treatment in [16]. This would serve as a simple model of a backreacted Kerr-like geometry that is accreting mass, and for which an analytic derivation of its shadow geometry is possible. For readers familiar with exact solutions in GR, a natural candidate would be the Kerr-Vaidya solution [17] which can be obtained by replacing the constant Kerr mass with a variable mass function in the original Kerr line element expressed in Eddington-Finkelstein coordinates. Unfortunately, as we'll elaborate later, this solution does not offer any additional Carter constant that could lead to its null geodesic equations being separable.

We construct our solutions by applying the Newman-Janis algorithm [18] to a spherically symmetric seed metric conformal to the Vaidya solution with the mass function that is linear in Eddington-Finkelstein coordinates. Fortunately, this solution-generating technique turns out to preserve the conformal Killing vector field in the original Vaidya metric, leading to separability of null geodesics, and ultimately allows us to develop an analytic formula for the boundary curve of its shadow. The solution space is parametrized by $\{a, \mu, M_s\}$ where $\{a, M_s\}$ are the spin and mass parameters of Kerr spacetime in the vanishing μ limit. Like the Kerr solution, there are regions in the moduli space which do not pertain to black holes. Motivated by phenomenological interests, we focus on the regime of parameters where our solution has event horizons like those of Kerr, with the conformal Killing horizon at a large distance away from the shadow observer and the outer horizon. Thus, our solution serves as a simple model of an accreting Kerr-like geometry not globally but for a finite spatial domain defined by the interior of the conformal Killing horizon. Generically, the shadow geometry is sensitive to the choice of coordinates. We work in a chart which reduces to the Kerr spacetime in Boyer-Lindquist coordinates in the limit $\mu = 0$, and the Vaidya spacetime in Eddington-Finkelstein-like coordinates in the limit $a = 0$. Correspondingly, we verified that our shadow formulas reduce consistently to those of Kerr [19] and Vaidya [16] under these limits.

As reviewed in for example [6], analytic derivations in cases that allow them complement numerical studies of shadow geometry in general. For example, for Schwarzschild spacetime, the angular diameter of its shadow is $\sim 3\sqrt{3}M_s/R_o$ for a distant observer located at the radial coordinate R_o [20]. This numerical value has turned out to be very useful as a guide in the analysis of shadow size and shape in EHT's recent observations [1, 2]. For our shadow analysis here, we find a simple power law describing the dependence of the mean radius and asymmetry factor of the shadow on

the accretion rate. The latter describes the departure of the shadow from circularity and has been constrained in M87* studies by EHT team [1]. When applied to the parameters of M87* and Sgr A*, our analysis of shadow geometry appears to indicate that the effect of μ is very small, and thus provides support for the assumption of using the pure Kerr metric throughout in GRMHD simulations. Our results, in addition, yield an empirical formula that parametrizes the variation of mean radius and asymmetry factor with accretion rate explicitly, and can thus be used to anticipate when backreaction of accretion on the metric may be significant.

Our paper is organized as follows. In Section 2, we present the construction of a class of Kerr-Vaidya-like solutions and elaborate on some basic aspects of its geometry and moduli space, followed by a derivation of some analytical formulas for shadow geometry in Section 3. In Section 4, we present several visual plots of the shadow and examine how the mean radius and asymmetry factor of the shadows vary with various parameters. We also include a brief discussion on recent EHT observations of M87* and Sgr A* in relation to our model geometry. Finally, we end with some concluding remarks in Section 5. Appendix A presents an extension of our solution obtained by matching the spacetime at some cutoff distance to Kerr-like solutions that are asymptotically flat via Darmois-Israel junction conditions. In Appendix B, for completeness, we develop an aberration formula for observers in another reference frame which, in the zero spin limit, reduces to another class of observers discussed previously in [16] for Vaidya spacetime.

2 A family of rotating Vaidya-like black hole solutions

We begin with the Vaidya metric in the coordinatesⁱⁱ

$$ds^2 = -\left(1 - \frac{2m(v)}{w}\right) dv^2 + 2dvdw + w^2 (d\theta^2 + \sin^2 \theta d\phi^2), \quad (1)$$

with the domains $v \in (0, \infty)$, $w \in (0, \infty)$, $\theta \in (0, \pi)$, $\phi \in (0, 2\pi)$. We note that $m(v)$ is a mass function that can be used to model a time-dependent black hole of which exterior is described by (1). The solution (1) solves the field equations in ordinary GR with the energy momentum tensor $T^{\mu\nu} = m(v)K^\mu K^\nu$, $K^\nu \partial_\nu = \partial_w$ which is typically interpreted as that of a null dust moving in the direction of decreasing w , with the black hole accreting (radiating) mass if $m'(v)$ is positive (negative).

2.1 Conformal factors, coordinate charts and the Newman-Janis algorithm

In this work, we restrict ourselves to the case where $m(v) = \mu v$, where μ is a positive constant. In this case, the geometry admits a conformal Killing vector field. To see this, we define ∂/∂_T as the conformal Killing vector and make a coordinate transformation as follows.

$$v = r_0 e^{T/r_0}, \quad w = r e^{T/r_0}, \quad (2)$$

where r_0 is a positive constant with dimension of length. This brings (1) to

$$ds^2 = e^{2T/r_0} \left(-\left(1 - \frac{2\mu r_0}{r} - \frac{2r}{r_0}\right) dT^2 + 2dTdr + r^2(d\theta^2 + \sin^2 \theta d\phi^2) \right), \quad (3)$$

ⁱⁱThe unusual choice of the symbol w to denote radial distance for this line element is solely due to shortage of conventions for the many different radial coordinates that we'll use throughout this paper.

with $T \in (-\infty, \infty)$, $r \in (0, \infty)$. In this form, the metric is conformal to a manifestly static spacetime which can be taken to generate a rotating solution via Newman-Janis algorithm. But first, we seek a temporal coordinate such that constant time slices are 3-dimensional spatial manifolds. Defining

$$T = t + \Upsilon(r), \quad \Upsilon(r) = \int^r d\tilde{R} \left(1 - \frac{2\mu r_o}{\tilde{R}} - \frac{2\tilde{R}}{r_0} \right)^{-1}, \quad (4)$$

the line element then reads

$$ds^2 = e^{\frac{2(t+\Upsilon(r))}{r_0}} \left(- \left(1 - \frac{2\mathcal{M}(r)}{r} \right) dt^2 + \left(1 - \frac{2\mathcal{M}(r)}{r} \right)^{-1} dR^2 + r^2(d\theta^2 + \sin^2\theta d\phi^2) \right) \equiv \Omega^2(t, r) ds_{static}^2, \quad (5)$$

where $t \in (-\infty, \infty)$ and

$$\mathcal{M}(r) \equiv \mu r_0 + \frac{r^2}{r_0}.$$

If we restrict ourselves to the spacetime patch where the conformal Killing vector field $\frac{\partial}{\partial t}$ is timelike, then letting $1 - 2\mathcal{M}/r > 0$ leads to the domain

$$r \in (R_h, R_c), \quad R_{h,c} = \frac{r_0}{4} \left(1 \pm \sqrt{1 - 16\mu} \right), \quad \mu < 1/16,$$

where R_h is the black hole horizon and R_c denotes the conformal Killing horizon. The Schwarzschild limit can be obtained as a double scaling limit as follows.

$$\mu \rightarrow 0, \quad r_0 \rightarrow \infty, \quad \mu r_o = M_s, \quad (6)$$

where M_s is a finite mass parameter equivalent to the ADM mass of the limiting Schwarzschild black hole. We now apply the Newman-Janis algorithmⁱⁱⁱ to the metric ds_{static}^2 which leads to a metric endowed with angular momentum

$$\begin{aligned} ds_{static}^2 \rightarrow ds_{rotating}^2 = & - \left(1 - \frac{2\mathcal{M}(r)r}{\Sigma} \right) dt^2 - \frac{4\mathcal{M}(r)ar \sin^2\theta}{\Sigma} d\phi dt \\ & + \left(r^2 + a^2 + \frac{2\mathcal{M}(r)a^2r \sin^2\theta}{\Sigma} \right) \sin^2\theta d\phi^2 + \frac{\Sigma}{\Delta} dr^2 + \Sigma d\theta^2, \end{aligned} \quad (7)$$

where a is the spin parameter and

$$\Sigma = r^2 + a^2 \cos^2\theta, \quad \Delta = r^2 - 2\mathcal{M}(r)r + a^2.$$

We will also modify the exponential argument of the conformal factor $\Omega(t, r)$ in (5) as follows

$$t + \Upsilon(r) \rightarrow t + \Upsilon_a(r), \quad \Upsilon_a(r) \equiv \int^r dr \frac{r^2 + a^2}{r^2 - 2\mathcal{M}(r)r + a^2}. \quad (8)$$

The full metric then reads

$$ds^2 = e^{\frac{2(t+\Upsilon_a(r))}{r_0}} ds_{rotating}^2, \quad (9)$$

with $ds_{rotating}^2$, $\Upsilon_a(r)$ being defined in (7) and (8) respectively. In the scaling limit of (6), the line element (9) reduces to Kerr spacetime in Boyer-Lindquist coordinates.

ⁱⁱⁱTo be precise, this algorithm carries with it the assumption of asymptotic flatness in the generated metric which doesn't hold for our solution though.

Now, like the Kerr solution where \mathcal{M} is instead just a constant, the metric (9) has singularities at the roots of $\Delta = 0$. To extend the spacetime beyond these singularities, we can perform a coordinate transformation

$$\tilde{T} = t + \Upsilon_a(r), \quad \tilde{\phi} = -\phi - a \int^r dr \frac{1}{r^2 - 2\mathcal{M}(r)r + a^2} \quad (10)$$

which leads to

$$ds^2 = e^{\frac{2\mu}{M_s}\tilde{T}} \left[- \left(1 - \frac{2\mathcal{M}(r)r}{r^2 + a^2 \cos^2 \theta} \right) (d\tilde{T} + a \sin^2 \theta d\tilde{\phi})^2 + 2(d\tilde{T} + a \sin^2 \theta d\tilde{\phi})(dr + a \sin^2 \theta d\tilde{\phi}) + (r^2 + a^2 \cos^2 \theta) d\Omega^2 \right], \quad (11)$$

In the $a = 0$ limit, we recover Vaidya spacetime in the conformally static coordinates of (3), whereas the $\mu = 0$ limit (as in (6)) takes the metric to that of Kerr in ingoing Eddington-Finkelstein coordinates. We note that in (11), replacing $\mathcal{M}(r) \rightarrow \mu\tilde{T}$ and removing the conformal factor $e^{\frac{2\mu}{M_s}\tilde{T}}$ yields the Kerr-Vaidya solution [17] which evidently isn't equipped with the conformal Killing symmetry. This leads to non-separability of null geodesics which would not allow us to solve for the shadow boundary curve analytically.

Our main interest in this class of time-dependent solutions lies in its property of being locally deformable to the Kerr geometry in Boyer-Lindquist coordinates in the $\mu \rightarrow 0, \mu r_0 \rightarrow M_s$ limit, and, in the limit of $a = 0$, to the Vaidya solution in a chart where it's conformally static. *This gives us a model of local geometry that approximates both spacetimes in a coordinate system suitable for deriving the analytical form of the black hole shadow.* For this specific purpose, we work in the $\{t, r, \theta, \phi\}$ chart (line element in (9)), where the spacetime is conformal to a Kerr-like solution in Boyer-Lindquist coordinates. In Section 2.2, we explore the parameter space $\{a, \mu, M_s\}$ in greater detail.

2.2 Horizons in the solution parameter space

In (9), setting $g^{rr} = 0$ yields the following cubic equation in r .

$$-\frac{2\mu}{M_s}r^3 + r^2 - 2M_s r + a^2 = 0. \quad (12)$$

In certain regimes of the parameter space of $\{\mu, a\}$, one could find event horizons. Consider the root space of the cubic equation (12) of which discriminant reads (henceforth, we define $a \rightarrow a/M_s$ to be a dimensionless parameter)

$$\mathfrak{D} = 4(1 - a^2 - 16\mu + 18a^2\mu - 27a^4\mu^2).$$

The sign of \mathfrak{D} determines the number of real roots to $g^{rr} = 0$. As a quadratic equation in μ , we can derive the curves along which $\mathfrak{D} = 0$, which read

$$\mu_{\pm} = \frac{-8 + 9a^2 \pm (4 - 3a^2)^{3/2}}{27a^4}. \quad (13)$$

They enclose the region which pertains to three distinct roots — two event horizons (outer and inner) and the conformal Killing horizon, and they intersect at the point (see Fig. 1)

$$(a_e, \mu_e) = \left(\frac{2}{\sqrt{3}}, \frac{1}{12} \right), \quad (14)$$

which represents a generalized extremal limit. At any constant $\mu \in (0, \frac{1}{12})$, the upper bound on a is given by taking $\mu = \mu_-(a)$ along which the inner and outer event horizons coincide. Along $\mu = \mu_+(a)$, the conformal Killing horizon coincides with the outer event horizon.

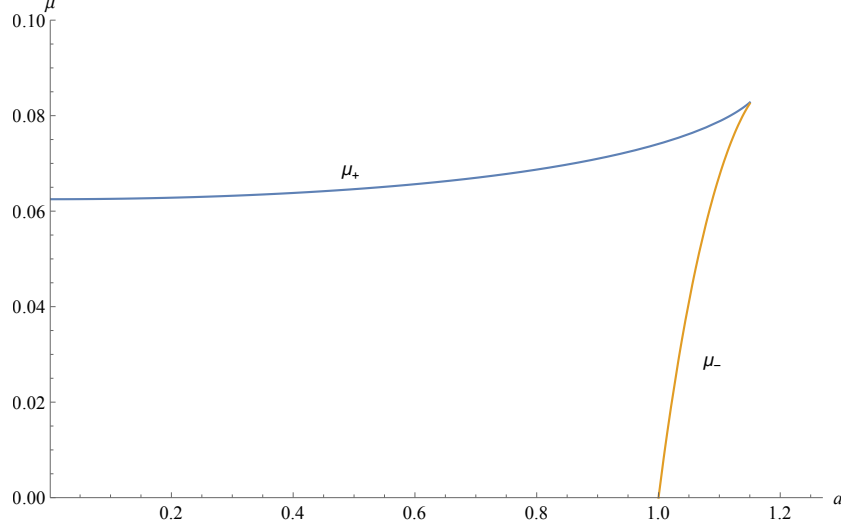


Figure 1: Graph depicting the parameter space (μ, a) of our family of solutions. The curve μ_+ begins at $(0, \frac{1}{16})$ and contains solutions where the outer event horizon and conformal Killing horizon are degenerate. The curve μ_- contains all the extremal solutions with degenerate outer and inner event horizons and with a finite conformal Killing horizon radius. Both curves merge at the extremal point $(\frac{2}{\sqrt{3}}, \frac{1}{12})$ at which there is only apparent horizon at $r = 2M_s$. Our family of solutions can be seen as parametric deformations of the Vaidya solution (vertical axis) and the Kerr solution (horizontal axis).

As depicted in Fig. 1, the region enclosed by the axes and the two curves has non-degenerate outer, inner event horizons and conformal Killing horizon. The small $\mu \ll 1$ region of this enclosed segment is of closer phenomenological interest to us. Let us consider a generic point in this region. Ordering the roots of (12) as $R_i < R_e < R_a$, we find that up to first few orders in μ, a :

$$\begin{aligned} R_e &= M_s \left(\left(1 + \sqrt{1 - a^2}\right) + \frac{4 + 4\sqrt{1 - a^2} - 5a^2 - 3a^2\sqrt{1 - a^2} + a^4}{2(1 - a^2)}\mu + \mathcal{O}(\mu^2) \right) \\ &= M_s [(2 + 8\mu) - (2\mu + 1/2)a + \dots] \end{aligned} \quad (15)$$

$$\begin{aligned} R_i &= M_s \left(\left(1 - \sqrt{1 - a^2}\right) + \frac{4 - 4\sqrt{1 - a^2} - 5a^2 + 3a^2\sqrt{1 - a^2} + a^4}{2(1 - a^2)}\mu + \mathcal{O}(\mu^2) \right) \\ &= M_s \left(\frac{a}{2} + \frac{a^2}{8} - \frac{\mu a^3}{16} + \frac{a^3}{16} + \dots \right) \end{aligned} \quad (16)$$

$$R_a = \frac{M_s}{2\mu} - 2M_s - 8\mu M_s + 2a\mu M_s + \dots \quad (17)$$

The radii R_e, R_i are those of the outer and inner event horizons smoothly connected to their corresponding expressions in the ordinary Kerr solution, whereas R_a is the radius of the conformal Killing horizon associated with the conformal Killing vector ∂_t (this symmetry is preserved by the Newman-Janis algorithm we implemented). For a generic point within our domain of interest (region enclosed by curves and axes in Fig. 1), our shadow observer is a timelike observer located at some distance $R_e < r < R_a$ away from the outer event or conformal Killing horizon.

3 Null geodesics, photon spheres and shadow formulas

3.1 On null geodesics

Metrics of the form $ds_{rotating}^2$ in (9) admit null geodesics which are separable. This condition was shown for the Kerr solution in for example [6, 19], and for other well-motivated forms of mass function $\mathcal{M}(r)$ in [21]. Such a property is preserved within its conformal class, and in particular by our line element ds^2 in (9). To appreciate this, we first recall that for a pair of metrics which are conformally related, say $g_{\mu\nu} = \Omega^2(x)\tilde{g}_{\mu\nu}$, their geodesic equations are related by

$$\frac{d^2x^\alpha}{d\eta^2} + \Gamma_{\beta\nu}^\alpha \frac{dx^\beta}{d\eta} \frac{dx^\nu}{d\eta} = 0 = \frac{d^2x^\alpha}{d\eta^2} + \tilde{\Gamma}_{\beta\nu}^\alpha \frac{dx^\beta}{d\eta} \frac{dx^\nu}{d\eta} - 2\Omega^{-1} \frac{d\Omega}{d\eta} \frac{dx^\alpha}{d\eta}, \quad (18)$$

where $\tilde{\Gamma}_{\beta\nu}^\alpha$ are the Christoffel symbols associated with the metric \tilde{g} . The last term of (18) can be rewritten as

$$\frac{d^2x^\alpha}{d\lambda^2} + \tilde{\Gamma}_{\beta\nu}^\alpha \frac{dx^\beta}{d\lambda} \frac{dx^\nu}{d\lambda} = 0, \quad \frac{d\lambda}{d\eta} = \Omega^2(x^\alpha(\eta)). \quad (19)$$

Thus, a suitable redefinition of the affine parameter leads to identical forms of the geodesic equations for the pair of conformally related metrics. In particular, we expect separability of null geodesic equations just like the Kerr solution or more generally the Kerr-like solutions studied in [21].

Our solution has a conformal Killing vector field $K \sim \partial_t$ which naturally gives a quantity conserved along its null geodesics. In parallel with the notion of energy in the static case, we call this conserved quantity $E = K^\mu P_\mu$. Also, the metric components are independent of ϕ , and we call $L = p_\phi$ the associated conserved quantity. These symmetries motivate the use of the Hamilton-Jacobi formalism for geodesics where one first defines an auxiliary action $S(\kappa, x^\mu)$ obeying

$$\frac{\partial S}{\partial \kappa} + \frac{1}{2} g_{\mu\nu} p^\mu p^\nu = 0, \quad p^\mu = g^{\mu\nu} p_\nu = g^{\mu\nu} \frac{\partial S}{\partial x^\nu}. \quad (20)$$

By virtue of the nature of conserved quantities, we adopt the following ansatz for the action S :

$$S = -\tilde{E}t + L\phi + S_r(r) + S_\theta(\theta) + \frac{1}{2}\mu^2\kappa, \quad \mu = -p_\alpha p^\alpha. \quad (21)$$

By construction, the 4-momenta $p^\mu = \frac{dx^\mu}{d\eta} = g^{\mu\nu} \partial_\nu S(x)$ satisfies the geodesic equation, with $\kappa = 0$ for null geodesics. We find that the Hamilton-Jacobi equation (20) leads to

$$-\Delta(r)(\partial_r S_r)^2 + [(r^2 + a^2)E - aL]^2/\Delta(r) = (\partial_\theta S_\theta)^2 + (L - aE \sin^2 \theta)^2/\sin^2 \theta = \mathcal{K}, \quad (22)$$

where the constant \mathcal{K} indicates separability. For deriving the shadow formulas, we need the explicit expressions for the 4-momenta which we find to simplify as

$$\frac{dt}{d\eta} = \frac{1}{\Sigma(r)} e^{-\frac{2(t+\Upsilon_a(r))}{r_0}} \left(-a(aE \sin^2 \theta - L) + \frac{(r^2 + a^2)P(r)}{\Delta(r)} \right), \quad (23)$$

$$\frac{dr}{d\eta} = \pm \frac{1}{\Sigma(r)} e^{-\frac{2(t+\Upsilon_a(r))}{r_0}} \sqrt{\mathcal{R}(r)}, \quad (24)$$

$$\frac{d\theta}{d\eta} = \pm \frac{1}{\Sigma(r)} e^{-\frac{2(t+\Upsilon_a(r))}{r_0}} \sqrt{\Xi(\theta)}, \quad (25)$$

$$\frac{d\phi}{d\eta} = \frac{1}{\Sigma(r)} e^{-\frac{2(t+\Upsilon_a(r))}{r_0}} \left(- \left(aE - \frac{L}{\sin^2 \theta} \right) + aP(r)/\Delta(r) \right), \quad (26)$$

where

$$P(r) \equiv E(r^2 + a^2) - aL, \quad \mathcal{R}(r) \equiv P(r)^2 - \mathcal{K}\Delta(r), \quad \Xi(\theta) \equiv \mathcal{Q} + \cos^2 \theta (a^2 E^2 - L^2 / \sin^2 \theta),$$

with \mathcal{Q} being conventionally called the Carter constant defined by

$$\mathcal{Q} \equiv \mathcal{K} - (L - aE)^2. \quad (27)$$

At this point, we note that apart from the specific form of our mass function $\mathcal{M}(r) = M_s + r^2/r_0$ implicitly contained in $\Delta(r) = r^2 - 2\mathcal{M}(r)r + a^2$, the 4-momenta expressions in (23) - (26) are identical to those found in [21] up to the conformal factor $e^{-\frac{2(t+\Upsilon_a(r))}{r_0}}$. This is consistent with the general relations governing conformally related metrics as described in eqns (18) and (19).

3.2 Shadow formulas from photon region

For our analysis of the shadow, we define the constants of motion

$$\eta \equiv \frac{\mathcal{Q}}{E^2}, \quad \xi \equiv \frac{L}{E}. \quad (28)$$

Any null geodesics with $r = R_p$ for some constant R_p leads to the condition

$$\mathcal{R}(R_p) = P(R_p)^2 - \mathcal{K}\Delta(R_p) = 0.$$

Further, if the orbit is unstable then setting $d^2r/d\eta^2 = 0$ yields

$$\mathcal{R}'(r_p) = 0.$$

After some algebra, we find that these couple of equations lead to the constants of motion

$$a \frac{L}{E} / M_s^2 = \frac{4(1 + \mu R_p^2)R_p^2 - (3\mu R_p^2 + R_p + 1)(R_p^2 + a^2)}{-3\mu R_p^2 - 1 + R_p}, \quad (29)$$

$$\frac{\mathcal{K}}{E^2} / M_s^2 = \frac{((R_p^2 + a^2) - aL/E)^2}{R_p^2 - 2(1 + \mu R_p^2)R_p + a^2}. \quad (30)$$

These constants of motion also characterize non-spherical geodesics which asymptotically approach those confined to spheres defined by $\mathcal{R}(R_p) = \mathcal{R}'(R_p) = 0$. In eqns. (29) and (30), and henceforth, for notational simplicity, we define R_p, a in units of M_s . Now consider an observer at the position (R_o, θ_{inc}) and described by an orthonormal tetrad as follows.

$$\begin{aligned} e_0 &= e^{-\frac{\mu T}{M_s}} \frac{(r^2 + a^2)\partial_t + a\partial_\phi}{\sqrt{\Sigma\Delta}}, \quad e_1 = e^{-\frac{\mu T}{M_s}} \sqrt{\frac{1}{\Sigma}} \partial_\theta, \\ e_2 &= -e^{-\frac{\mu T}{M_s}} \frac{\partial_\phi + a \sin^2 \theta \partial_t}{\sqrt{\Sigma} \sin \theta}, \quad e_3 = -e^{-\frac{\mu T}{M_s}} \sqrt{\frac{\Delta}{\Sigma}} \partial_r. \end{aligned} \quad (31)$$

As explained in for example [6, 19], this choice leads to e_0 being the 4-velocity of the shadow observer with $e_0 \pm e_3$ being tangential to the principal null congruences. (The various expressions in (31) differ from those in [6, 19] by the conformal factor which we need to take into account for an orthonormalized set of basis vectors.) The tangent vector of each light ray reaching the observer reads

$$\frac{d}{d\eta} = p^\mu \partial_\mu = \dot{r} \partial_r + \dot{\theta} \partial_\theta + \dot{\phi} \partial_\phi + \dot{t} \partial_t = \alpha(-e_0 + \sin \theta \cos \phi e_1 + \sin \theta \sin \phi e_2 + \cos \theta e_3), \quad (32)$$

where $\alpha = g_{\mu\nu}p^\mu e_0^\nu$. Equating the coefficients after evaluating both sides of (32) at (R_o, θ_{inc}) yields

$$\sin \Phi = \frac{L_E(R_p) - a \sin^2 \theta_{inc}}{\sqrt{\mathcal{K}_E(R_p)} \sin \theta_{inc}}, \quad \sin \Theta = \frac{\sqrt{\Delta(R_o)} \mathcal{K}_E(R_p)}{R_o^2 - a L_E(R_p) + a^2}, \quad (33)$$

where

$$L_E \equiv \frac{L}{M_s^2 E}, \quad \mathcal{K}_E \equiv \frac{\mathcal{K}}{M_s^2 E^2},$$

and we have switched to a different notation for the celestial coordinates Φ, Θ for clarity having derived their eventual expressions. In particular, we note that θ_{inc} measures the angle between the black hole's spin axis as defined by $\theta = 0$ (the zero locus of $g_{\phi\phi}$) and the observer, with e_3 being parallel to the line of sight connecting the observer to the origin of the Boyer-Lindquist-like chart in (9).

The photon region consists of spherical orbits with radii bounded in the domain

$$R_p \in (R_{p,min}, R_{p,max}), \quad (34)$$

where $R_{p,min}, R_{p,max}$ are defined by setting $\sin \Phi = +1, -1$ respectively, i.e.

$$a L_E(R_{p,min}) = a^2 \sin^2 \theta_{inc} + a \sqrt{\mathcal{K}_E(R_{p,min})} \sin(\theta_{inc}), \quad (35)$$

$$a L_E(R_{p,max}) = -a^2 \sin^2 \theta_{inc} - a \sqrt{\mathcal{K}_E(R_{p,max})} \sin(\theta_{inc}). \quad (36)$$

In the vanishing a limit, the width of the photon region $(R_{p,min}, R_{p,max})$ goes to zero, and collapses to a single value of R_p which is the photon sphere radius of Vaidya spacetime. In this limit, from (35),

$$\lim_{a \rightarrow 0} a L_E \rightarrow R_p^2 \frac{3 + \mu R_p^2 - R_p}{R_p - 1 - 3\mu R_p^2} = 0 \Rightarrow R_p = \frac{1}{2\mu} \left(1 - \sqrt{1 - 12\mu} \right),$$

where we have restricted the root to be smaller than the conformal Killing horizon radius. This is indeed the expression obtained in [16]. Further taking the $\mu = 0$ limit yields $R_p = 3$ which is the radius of Schwarzschild photon sphere. In the $a = 0$ limit, our expression for $\sin \Theta$ in (33) reduces to eqn. (41) of [16] which is the sine of the angular radius of the Vaidya solution's shadow.

4 Portraits of the shadow

In this Section, we discuss geometrical properties of the shadow in more details. We first recall that the coordinate system describing the shadow observer has a conformal Killing horizon R_a obtained as the largest root of $g^{rr} = 0$ in the line element (9) which we reproduce explicitly below for convenience.

$$ds^2 = e^{\frac{2(t+\Upsilon_a(r))}{r_0}} \left[- \left(1 - \frac{2\mathcal{M}(r)r}{\Sigma} \right) dt^2 - \frac{4\mathcal{M}(r)ar \sin^2 \theta}{\Sigma} d\phi dt + \left(r^2 + a^2 + \frac{2\mathcal{M}(r)a^2 r \sin^2 \theta}{\Sigma} \right) \sin^2 \theta d\phi^2 + \frac{\Sigma}{\Delta} dr^2 + \Sigma d\theta^2 \right], \quad (37)$$

where $\mathcal{M}(r) = M_s + \frac{r^2}{r_0}$ and $\Upsilon_a(r) \equiv \int^r dr \frac{r^2 + a^2}{r^2 - 2\mathcal{M}(r)r + a^2}$. For our shadow observer located at some radial distance R_o , we would also like $g_{tt} < 0$ for all values of θ , leading to the condition

$$R_h < R_o < R_c < R_a, \quad R_{h,c} = \frac{r_0}{4} \left(1 \mp \sqrt{1 - 16\mu} \right), \quad (38)$$

where R_h, R_c are the event and Killing horizons of the Vaidya solution in the $a = 0$ limit. This also implies that for some fixed R_o , we have an upper bound on

$$\mu < \mu_b \equiv M_s \frac{R_o - 2M_s}{2R_o^2}, \quad (39)$$

since we wish to have $R_o < R_c$. For the visual representation of the shadow, we follow the convention used by Johannsen and Psaltis in [13]. This is essentially the orthonormal tetrad we used in deriving the shadow formula, with the x, y coordinates being

$$x = R_o \sin(\Theta(R_p, R_o)) \sin(\Phi(R_p, \theta_{inc})), \quad (40)$$

$$y = \pm R_o \sin(\Theta(R_p, R_o)) \cos(\Phi(R_p, \theta_{inc})). \quad (41)$$

These coordinates parametrize the observer's plane upon which the shadow is projected.^{iv} From (33), noting that L_E and \mathcal{K}_E are odd and even in the spin parameter a respectively, one can straightforwardly identify the discrete symmetry

$$a \rightarrow -a, \quad \theta_{inc} \rightarrow -\theta_{inc},$$

which implies in particular that $a < 0$ shadows can be obtained from their $a > 0$ counterparts by a reflection in the y -axis (for all our shadow plots, we take $a > 0$).

In quantifying the shape of the shadow, we follow the work of Johannsen and Psaltis in [13] who introduced the asymmetry parameter \mathcal{A} to describe departure from circularity.

$$\mathcal{A} = 2 \sqrt{\frac{\int_0^{2\pi} d\alpha (R - \bar{R})^2}{\int_0^{2\pi} d\alpha}}, \quad \tan \alpha = \frac{y}{x}, \quad R \equiv \sqrt{(x - D)^2 + y^2}, \quad D \equiv \frac{|x_{max} + x_{min}|}{2}, \quad (42)$$

and $\bar{R} = \int_0^{2\pi} d\alpha R / 2\pi$ is the averaged radius projected upon the observer's plane. These quantities were mentioned in the EHT paper [1] for M87*, and we checked that our shadow geometries for the background Kerr solution (with $\mu = 0$) yield comparable features obtained previously in the work of Johannsen and Psaltis [13]. In Figure 2, we picked a few values of a, θ_{inc} for a black hole located at some R_o to demonstrate how the shadow curve changes with μ .

4.1 Scaling laws for variation of \bar{R} and \mathcal{A} with μ

The parameter space for the shadow geometry is spanned by $\{a, \theta_{inc}, R_o, \mu\}$. Computing the shadow's mean radius and asymmetry factor for a range of parameters, we find a simple empirical scaling law that describes the variation of \bar{R}, \mathcal{A} with the accretion rate parameter μ and other parameters as follows.

$$\bar{R} = \bar{R}_o(a, \theta_{inc}, R_o) \sqrt{1 - \frac{\mu}{\mu_b(R_o)}}, \quad \bar{\mathcal{A}} = \bar{\mathcal{A}}_o(a, \theta_{inc}, R_o) \sqrt{1 - \frac{\mu}{\mu_b(R_o)}}, \quad (43)$$

where $\mu_b(R_o)$ is the upper bound (39) on the accretion rate allowed by our model for some fixed observer distance R_o , obtained by setting the conformal Killing horizon to be the observer distance.

^{iv} Another set of projection coordinates used for plotting the black hole shadow is the (α, β) parameters of Bardeen which would not be entirely suitable in our case since our solution is not asymptotically flat. See for example the review of [6] which discusses the relations between Bardeen's impact parameters and others such as stereographic coordinates, etc.

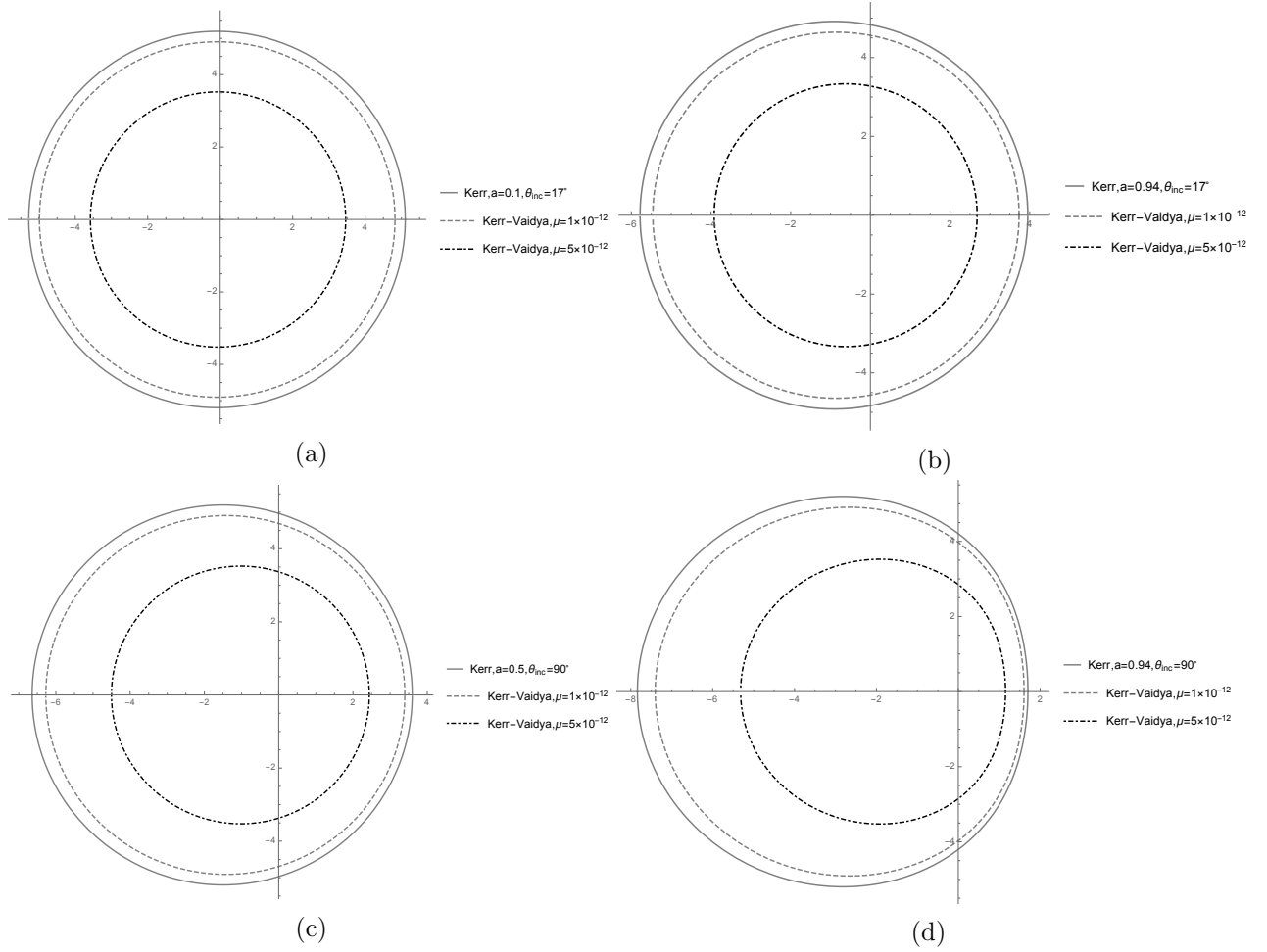


Figure 2: A visual representation of the shadow projected upon the observer plane at $R_o/M_s = 5.4 \times 10^{10}$ with $\theta_{inc} = 17^\circ$ for (a) and (b), $\theta_{inc} = 90^\circ$ in (c) and (d). The upper bound on $\mu_b \sim 9.26 \times 10^{-12}$. Horizontal axes are scaled in units of M_s .

The dependence on μ appears as a separate factor independent of the other shadow parameters, with the functions $\bar{R}_o(a, \theta_{inc}, R_o)$, $\bar{\mathcal{A}}_o(a, \theta_{inc}, R_o)$ describing the radius and asymmetry factor at $\mu = 0$. The form of (43) implies that for $\mu \ll 1$, $R_o \gg M_s$, the fractional decrease in the mean radius and the asymmetry factor that is induced by a non-zero μ scales approximately as

$$\frac{\delta \bar{R}}{\bar{R}} = \frac{\delta \mathcal{A}}{\mathcal{A}} \approx -\mu \frac{R_o}{M_s}. \quad (44)$$

In Figure 3, we plot these functions for a few values of spin at a fixed R_o and θ_{inc} . These plots are expectedly similar to the corresponding ones presented in [13] and [14]. At higher spin values, the asymmetry factor and mean radius exhibit a greater range of values over the θ_{inc} domain. At any θ_{inc} , increasing a increases $\bar{\mathcal{A}}_o$ but decreases \bar{R}_o . The form of (43) also implies that the asymmetry factor expressed in units of the mean radius is independent of μ , with

$$\frac{\mathcal{A}}{\bar{R}} = \frac{\bar{\mathcal{A}}_o}{\bar{R}_o}(a, \theta_{inc}, R_o). \quad (45)$$

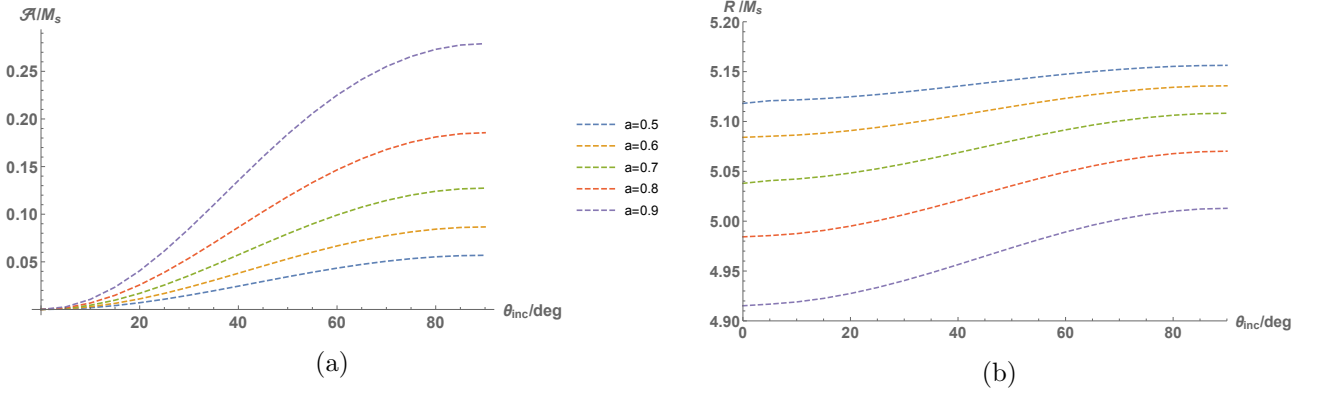


Figure 3: Graphs depicting how \bar{R}, \mathcal{A} vary with angle θ_{inc} , at $\mu = 0$. We plot the functions $\bar{R}_o(a, \theta_{inc}, R_o), \bar{\mathcal{A}}_o(a, \theta_{inc}, R_o)$ at five values of a at $R_o/M_s = 5.4 \times 10^{10}$ and $\theta_{inc} = 17^\circ$.

In Figures 4, 5 and 6, we plot the empirical fitting curves (described by (43)) that depict how \bar{R}, \mathcal{A} vary with the accretion parameter μ and each of the parameters $\{a, \theta_{inc}, R_o\}$ separately.

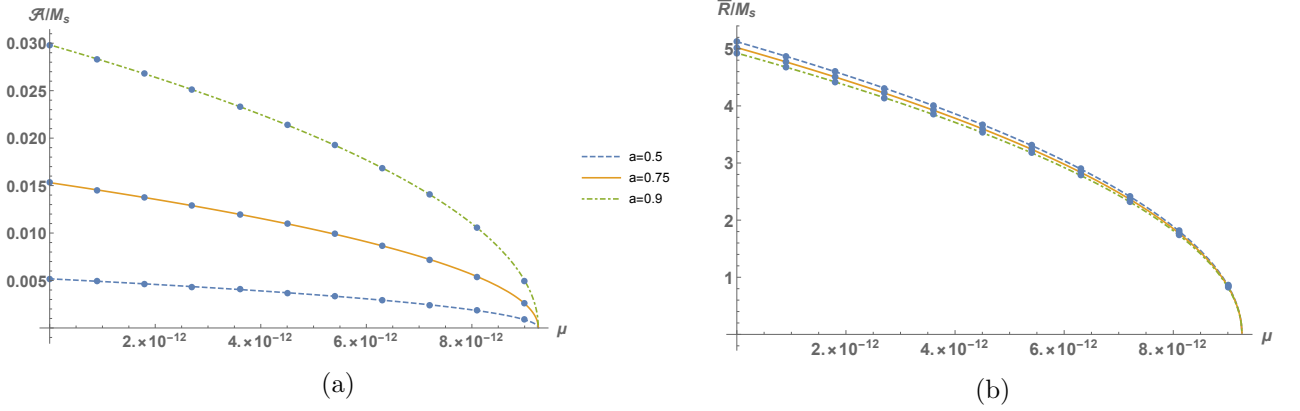


Figure 4: Graphs depicting how \bar{R}, \mathcal{A} vary with μ for $a = 0.5, 0.75, 0.9$, with $R_o/M_s = 5.4 \times 10^{10}, \theta_{inc} = 17^\circ$.

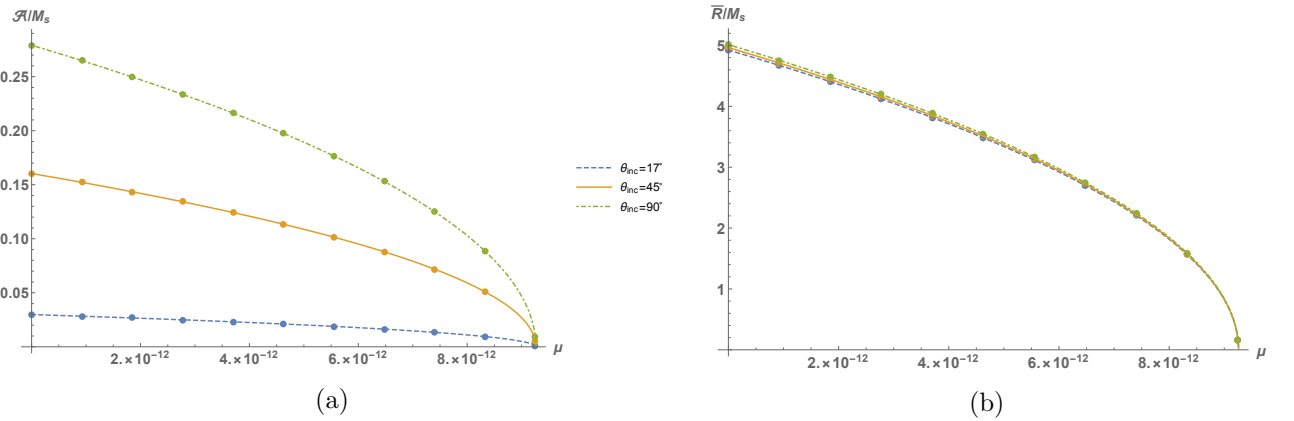


Figure 5: Graphs depicting how \bar{R}, \mathcal{A} vary with μ for $\theta_{inc} = 17^\circ, 45^\circ, 90^\circ$, with $R_o/M_s = 5.4 \times 10^{10}, a = 0.9$.

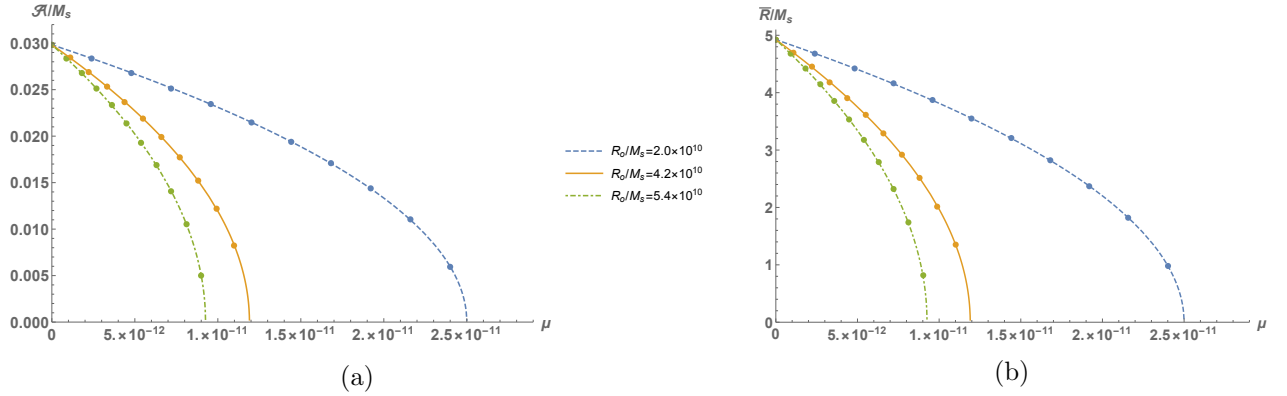


Figure 6: Graphs depicting how \bar{R}, \mathcal{A} vary with R_o for $R_o/M_s = 2.0 \times 10^{10}, 4.2 \times 10^{10}, 5.4 \times 10^{10}$ with $\theta_{inc} = 17^\circ$ and $a = 0.9$.

4.2 On the shadows of M87* and Sagittarius A* as observed by EHT

The M87* black hole was found to be about 16.8 Mpc away, with a mass $M_s \simeq 6.5 \times 10^9 M_\odot$ [1]. The ensemble of accretion models used by the EHT team [1, 7] involved mass rates that ranged from about 2×10^{-7} to 4×10^{-4} times the Eddington rate \dot{M}_{Edd} . In their work, $\dot{M}_{\text{Edd}} \sim 137 M_\odot/\text{yr}$, and we find that this translates into

$$\mu_{\text{M87}} = \dot{M} \times \frac{GM_\odot}{\text{Yr} \times c^2} \sim \dot{M} \times 1.56 \times 10^{-13} \in (4 \times 10^{-18}, 9 \times 10^{-15}),$$

where \dot{M} is mass rate in units of M_\odot/yr . This is smaller than the upper bound $\mu_b \sim 9.2 \times 10^{-12}$ for $R_o \sim 16.8$ Mpc. Equivalently, for this range of μ , the conformal Killing horizon size falls within

$$R_c/M_s \sim (5.9 \times 10^{13}, 1.16 \times 10^{17}),$$

which lies beyond $R_o/M_s \sim 5.4 \times 10^{10}$. Thus, the observed distance to M87* and estimates of mass accretion are well within the domains of validity of our simple model geometry. Now it was estimated in [22] that the angle of inclination is around 17° . Corresponding to this value, in Figure 7, we plot the variation of the shape parameters \bar{R}, \mathcal{A} and their ratio with the spin parameter a . The range of values of \bar{R} translates into the shadow angular diameter $\sim (36.9 \mu\text{as}, 39.6 \mu\text{as})$ which is comparable to the measured emission ring diameter in the EHT experiment [1]. The maximum \mathcal{A}/\bar{R} ratio is about 0.01 which is within limits of the upper bound of 10% indicated in [1]. The highest $\mu \sim 8.5 \times 10^{-15}$ in the ensemble of models considered in [1] translates only to a fractional shift of 0.05 % in \bar{R}, \mathcal{A} .

Sgr A* has been observed to located near the dynamical center of our galaxy at a distance $R_o \sim 8$ kpc away, with a dense concentration of mass $M_s \sim 4 \times 10^6 M_\odot$. In contrast to M87* where its prominent jet provides robust constraints on source orientation with respect to the line of sight, fixing it to be $\sim 17^\circ$, there is no such constraint unfortunately on Sgr A* [2]. However, GRMHD models appeared to have favored $\theta_{inc} < 50^\circ$, with accretion rate of order-of-magnitude $10^{-9} - 10^{-8} M_\odot \text{yr}^{-1}$. These models were equipped with spin parameter values of $a = 0.5, 0.94$ [2]. As mentioned in [2], in the earlier works of Quataert [23] and Baganoff [24], the captured accretion rate was estimated to be $10^{-6} - 10^{-5} M_\odot \text{yr}^{-1}$ from Chandra observations of thermal bremsstrahlung emission at the vicinity of the gas capture radius. Most recently, in [11], a promising model was identified in which $\theta_{inc} \leq 30^\circ$, and accretion models of $\dot{M} \sim 5.2 - 9.5 \times 10^{-9} M_\odot/\text{yr}$ were examined.

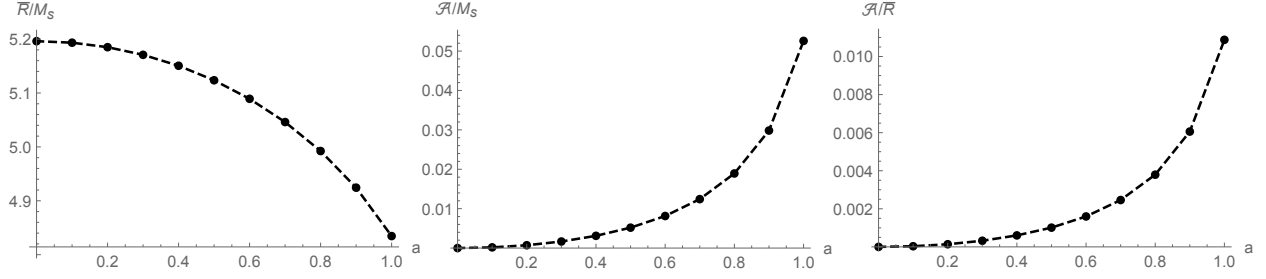


Figure 7: Graphs showing how the mean radius \bar{R} , asymmetry factor \mathcal{A} and their ratio vary with a , with $R_o/M_s = 5.4 \times 10^{10}$ (pertaining to EHT observation of M87*), $\theta_{inc} = 17^\circ$.

Even for the accretion rate $\dot{M} = 10^{-5} M_\odot \text{ yr}^{-1}$ this translates into merely

$$\mu_{sgr} \sim 1.6 \times 10^{-18}.$$

Like the case of M87*, this turns out to be smaller than the upper bound $\mu_b \sim 1.2 \times 10^{-11}$ for $R_o \sim 8$ kpc. Equivalently, taking this value of μ_{sgr} , the conformal Killing horizon size is

$$R_c/M_s \sim 3.2 \times 10^{17},$$

which lies beyond $R_o/M_s \sim 4.2 \times 10^{10}$. Thus again, both observer distance and (estimated) mass accretion rates are well within the domains of validity of our simple model geometry.

In Figure 8, we plot the variation of the shape parameters \bar{R} , \mathcal{A} and their ratio with the spin parameter a , at a few representative values of θ_{inc} . Over the domain of $\theta_{inc} \in (10^\circ, 50^\circ)$, the range of shadow angular diameters is $\sim (47.6 \mu\text{as}, 51.2 \mu\text{as})$ which is comparable to the shadow diameter estimate $48.7 \pm 7.0 \mu\text{as}$ in the EHT experiment [2]. The asymmetry factor-to-mean radius ratio \mathcal{A}/\bar{R} ratio increases with θ_{inc} , and can be as high as $\sim 10\%$ for $\theta_{inc} = 50^\circ$. It would be interesting to study this geometrical signature for the EHT's Sgr A* shadow image. In [8], the EHT team mentioned in passing that the sparse interferometric coverage of 2017 observations led to significant uncertainties in circularity measurements which were thus not quantified yet, but future EHT observations with additional telescopes may place constraints on the circularity. Finally, let us mention that the effect of μ on \bar{R} , \mathcal{A} is even smaller for Sgr A*, inducing only a fractional change of 10^{-6} in these quantities.

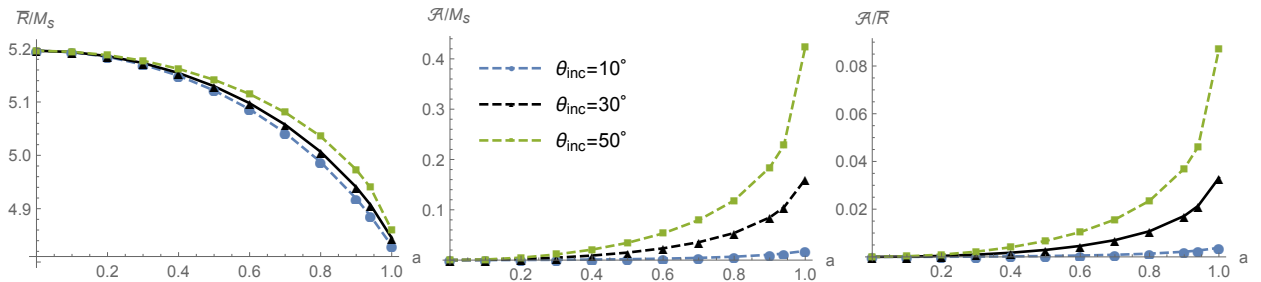


Figure 8: Graphs showing how the mean radius \bar{R} , asymmetry factor \mathcal{A} and their ratio vary with a , with $R_o/M_s = 4.2 \times 10^{10}$ (pertaining to EHT observation of Sgr A*), $\theta_{inc} = 10^\circ, 30^\circ, 50^\circ$.

5 Discussion

We have presented a study of the shadow geometry for a class of spacetime metric that is Kerr-Vaidya-like in nature. The family of time-dependent black hole solutions we constructed in this work has well-defined Kerr and Vaidya limits. Agnostic to the source and the underlying theory, we had conceived of its form starting from the Vaidya solution with a mass function that is linear in Eddington-Finkelstein coordinates since this particular class of solutions furnishes a model for accretion and is equipped with a conformal Killing isometry that leads to separability of null geodesics. After expressing it as being conformal to a solution that is Schwarzschild-like with a radial coordinate-dependent mass function, the Newman-Janis algorithm was applied to obtain a Kerr-like solution that reduces to the Kerr solution in the limit of vanishing accretion parameter μ . In real-life applications, the dimensionless accretion rate μ is expected to be very small, for instance, for the recent M87* and Sgr A* observations, the highest model estimates of μ are of the order $10^{-15}, 10^{-18}$ respectively. Thus, our model geometry can be considered as a small μ -deformation of the Kerr solution that preserves separability of null geodesics, or from a different perspective, a rotating generalization of the Vaidya solution. For a finite spatial domain, it could act as a simple model of a Kerr-like geometry that takes into account the backreaction of accretion. The existence of a conformal Killing vector field allows us to solve for the shadow geometry straightforwardly yet also brings with it the subtlety of a horizon that should be located beyond the shadow observer. Equivalently, at any fixed observer distance, there exists an upper bound to μ (eqn.(39)) for applicability of our model.

In our study of the variation of the mean radius \bar{R} and asymmetry factor \mathcal{A} with regards to various parameters — $\{\mu, a, \theta_{inc}, R_o\}$, we found a simple empirical scaling law of the form in (43). In particular, this implies that at small $\mu \ll 1$ and large observer distance $R_o \gg M_s$, the fractional change induced by turning on the accretion rate parameter μ reads simply as

$$\frac{\delta \bar{R}}{\bar{R}} = \frac{\delta \mathcal{A}}{\mathcal{A}} \approx -\mu \frac{R_o}{M_s}. \quad (46)$$

To our knowledge, we have not encountered any previous descriptive relations between shadow geometrical features and accretion rate, black hole and observer parameters of the form similar to (43) or (46)^v. GRMHD simulations (e.g. [10, 12, 26]) typically assume the validity of the background metric being purely Kerr in some suitable coordinate system, with the complicated astrophysics of accretion contained within the choice of the energy-momentum tensor. Even for GRMHD simulations involving spacetime metrics motivated by beyond-GR theories (e.g. [8]), the accretion parameter is rarely involved in describing the background spacetime. In [13, 14] and most recently in [15], it was found that the accretion details do not appear to influence the shadow geometry which is sensitive only to the background metric. The assumption here is that backreactions of accretion on the metric are insignificant. Indeed, in applying our model to EHT observations of M87* and Sgr A*, we found that the most generous estimates of μ in [1] and [2] yield fractional changes of \bar{R} and \mathcal{A} of the order of 10^{-4} and 10^{-6} respectively, consistent with such an assumption. In addition, our model yields an explicit relation in (43) that describes how, at least in principle, the shadow geometry changes with accretion rate. From (46), it may seem that for situations where the (fractional) experimental uncertainties $\delta \bar{R}_e / \bar{R}_e, \delta \mathcal{A}_e / \mathcal{A}_e$ are of the order $\mu R_o / M_s$, then metric

^vIn [25], it was found that increasing the flux of infalling gas into a Schwarzschild black hole (and hence the accretion rate) by increasing an axion-plasmon coupling parameter decreases the size of the shadow which qualitatively agrees with the variation of \bar{R} with μ of our model. It would be interesting to study if the results in [25] could be cast in a similar form as (43) or (46).

backreactions due to accretion may be important in analyzing geometrical details of the black hole shadow.

A limitation of our model geometry is that it is only asymptotically Ricci-flat and not Minkowskian. As a model of an effective Kerr-like geometry with accretion backreaction, it is thus valid only for a finite spatial domain. Imposing a stricter condition for $g_{tt} < 0$ in (37), in our exposition of the black hole shadow analysis, we have taken the observer location R_o to lie within the interior of the sphere defined by the conformal Killing horizon of the limiting Vaidya spacetime, i.e. $R < R_c$ in the coordinate system of (37). (For M87* and Sgr A*, $R_c/R_o \sim 10^3, 10^7$ respectively.) It would be interesting to seek a refinement of our model geometry in one that allows for separability of null geodesics while being asymptotically flat. Towards this ideal goal, in Appendix A, we sketched a globally well-defined solution obtained by matching the spacetime at some cutoff distance to asymptotically flat Kerr-like solutions using Darmois-Israel junction conditions, leaving more realistic constructions for future work.

Acknowledgments

I am grateful to Jan de Boer, Chong-Sun Chu, Ori Ganor, Petr Horava, Daniel Robbins and Neal Snyderman for sharing with me their insights on various aspects of gravitational physics and their moral support over the years.

A Global geometry and matching spacetimes via junction conditions

For the Vaidya spacetime, the conformally static chart in (3) has a coordinate singularity at the conformal Killing horizon. It can be continued beyond that via (2). Similarly, from (11), we can perform the coordinate transformation (2)

$$v = r_0 e^{\tilde{T}/r_0}, \quad w = r e^{\tilde{T}/r_0}, \quad (47)$$

after which the line element takes the form

$$\begin{aligned} ds^2 = & -F\left(\frac{w}{v}\right) \left(dv + \frac{av \sin^2 \theta}{r_0} d\tilde{\phi}\right)^2 + 2 \left(dv + \frac{av \sin^2 \theta}{r_0} d\tilde{\phi}\right) \left(dw + \frac{av \sin^2 \theta}{r_0} d\tilde{\phi}\right) \\ & - \frac{2aw \sin^2 \theta}{r_0} dv d\tilde{\phi} + \left(w^2 + \frac{v^2 a^2 \cos^2 \theta}{r_0^2}\right) d\Omega^2, \end{aligned} \quad (48)$$

where

$$F\left(\frac{w}{v}\right) = -1 + \frac{2\left(\mu + \left(\frac{w}{v}\right)^2\right) \frac{w}{v}}{\left(\frac{w}{v}\right)^2 + \frac{a^2 \cos^2 \theta}{r_0^2}} - \frac{2w}{v}.$$

The Vaidya metric in the chart (1) is obtained in the $a = 0$ limit, whereas the double scaling limit of (6) brings it to Kerr in Eddington-Finkelstein chart. The metric in the chart $\{v, w, \theta, \tilde{\phi}\}$ is convenient for examining the asymptotic infinity of the spacetime. Taking the limit of infinite w yields the following asymptotic form

$$\lim_{w \rightarrow \infty} ds^2 \sim -dv^2 + 2dv dw + w^2 d\Omega^2 + \frac{2a\mu}{M_s} \sin^2 \theta \left(w dv d\tilde{\phi} + v dw d\tilde{\phi}\right). \quad (49)$$

but with ds_K^2 defined as in (52). Next, at $\tilde{T} = \{\tilde{T}_i, \tilde{T}_f\}$, we cut-and-paste \mathcal{G} to $\mathcal{G}_i, \mathcal{G}_f$ respectively which are defined by

$$\mathcal{G}_i : ds^2 = ds_K^2(a^i, \mu, M_K^i, R_m^i), \quad \mathcal{G}_f : ds^2 = ds_K^2(a^f, \mu, M_K^f, R_m^f). \quad (54)$$

The initial and final matching surfaces are spacelike surfaces, and the various parameters are related as

$$e^{\frac{\tilde{T}_i}{r_0}} R_m = R_m^i, \quad e^{\frac{\tilde{T}_i}{r_0}} M_K = M_K^i, \quad e^{\frac{\tilde{T}_i}{r_0}} a = a^i, \quad (55)$$

$$e^{\frac{\tilde{T}_f}{r_0}} R_m = R_m^f, \quad e^{\frac{\tilde{T}_f}{r_0}} M_K = M_K^f, \quad e^{\frac{\tilde{T}_f}{r_0}} a = a^f. \quad (56)$$

The initial geometry can be taken to be arbitrarily close to Minkowski spacetime with $\tilde{T}_i \rightarrow -\infty$ with (R_m, M_K, a) being some finite set of parameters. The eventual geometry from the mass accretion process of duration $\Delta\tilde{T} = \tilde{T}_f - \tilde{T}_i$ is that of the Kerr solution (for $R > R_m^f$) with mass and spin parameters being

$$M_K^f = e^{\mu \frac{\Delta\tilde{T}}{M_s}} M_K^i, \quad a^f = e^{\mu \frac{\Delta\tilde{T}}{M_s}} a^i. \quad (57)$$

From (57), one can easily see that our model geometry manifestly represents an accretion process where the fractional increase in *both* the mass and spin parameters occur at a rate of μ .

B On the reference frame of the shadow observer

B.1 In the limit of $a = 0$

In the limit of $a = 0$, the tetrad basis (31) defining the reference frame of our shadow observer reduces to the following.

$$e_0 = \frac{e^{-\mu\tilde{T}/M_s}}{\sqrt{1 - \frac{2\mathcal{M}}{r}}} \partial_t, \quad e_1 = \frac{e^{-\mu\tilde{T}/M_s}}{r} \partial_\theta, \quad e_2 = -\frac{e^{-\mu\tilde{T}/M_s}}{r \sin \theta} \partial_\phi, \quad e_3 = -e^{-\mu\tilde{T}/M_s} \sqrt{\left(1 - \frac{2\mathcal{M}}{r}\right)} \partial_r \quad (58)$$

In the chart $\{\tilde{T}, r, \theta, \tilde{\phi}\}$, we replace $\partial_t \rightarrow \partial_{\tilde{T}}, \partial_r \rightarrow \frac{\partial\tilde{T}}{\partial r} \frac{\partial}{\partial\tilde{T}} + \frac{\partial}{\partial r}$ which leads to

$$e_0 = \frac{e^{-\mu\tilde{T}/M_s}}{\sqrt{f}} \partial_{\tilde{T}}, \quad e_1 = \frac{e^{-\mu\tilde{T}/M_s}}{r} \partial_\theta, \quad e_2 = -\frac{e^{-\mu\tilde{T}/M_s}}{r \sin \theta} \partial_\phi, \quad e_3 = -\frac{e^{-\mu\tilde{T}/M_s}}{\sqrt{f}} (\partial_{\tilde{T}} + f \partial_r) \quad (59)$$

where $f = 1 - \frac{2\mathcal{M}(r)}{r}$. This is the tetrad basis used in [16] for Vaidya spacetime's shadow calculation, relevant for an observer with 4-velocity e_0, ϕ, r .

B.2 Observers in the $\{v, w, \theta, \phi\}$ chart and aberration formulas

The coordinate system $\{v, w, \theta, \phi\}$ avoids the horizons as coordinate singularities. In [16], the shadow observed by an observer with 4-velocity $\sim \frac{\partial}{\partial v}$ was derived using an aberration formula being applied to the shadow angle formula.

In general, for a pair of reference frames (S, S') , aberration formulas relating the coordinates of their celestial spheres can be derived from the expression (32) after we express the 4-velocity e'_0 of the S' reference frame as a linear combination of the original tetrad basis components, writing

$$e'_0 = \frac{e_0 + V^k e_k}{\sqrt{1 - v^2}}, \quad (60)$$

where \vec{V} is the relative 3-velocity of S' observer. Consider an observer of which e'_0 is a linear combination of e_0 and another basis vector e_3 . Its tetrad basis components read

$$e'_0 = \frac{1}{\sqrt{1-V^2}}(e_0 + Ve_3), \quad e'_3 = \frac{1}{\sqrt{1-V^2}}(e_3 + Ve_0), \quad e'_{1,2} = e_{1,2}. \quad (61)$$

Taking the inner product between e'_0, e'_3 and the tangent vector expression in (32) in both unprimed and primed coordinates, we obtain the aberration formulas

$$\cos \theta' = \frac{V + \cos \theta}{1 + V \cos \theta}, \quad \phi' = \phi, \quad V = -\frac{e'_0 \cdot e_3}{e'_0 \cdot e_0}. \quad (62)$$

In [16], the observer with $e'_0 \sim \frac{\partial}{\partial v}$ was also considered. After a coordinate transformation from $\{\tilde{T}, r, \theta, \tilde{\phi}\}$ used for the tetrad basis in (59), one can show that

$$e'_0 \sim \frac{\partial}{\partial v} = \frac{1}{\sqrt{1 - \frac{2M_s}{r}}} e^{-\frac{r}{r_0}} \left(\partial_{\tilde{T}} - \frac{r}{r_0} \partial_r \right) = \frac{1}{\sqrt{1 - V^2}}(e_0 + Ve_3), \quad V = \frac{r^2}{r^2 + rr_0 \left(1 - \frac{2\mathcal{M}(r)}{r} \right)} \quad (63)$$

where e_0, e_1, e_2, e_3 are as defined in (59). In [16], the same expression for the relative velocity V was obtained with an aberration relation $\tan^2 \frac{\theta'}{2} = \frac{1-V}{1+V} \tan^2 \frac{\theta}{2}$ that we verified to be identical to (62).

Let us now consider an appropriate S' observer for our Kerr-Vaidya-like geometry. We note that for the S observer, its 4-velocity e_0 is a linear combination of $\partial_{\tilde{T}}$ and $\partial_{\tilde{\phi}}$, or in the Boyer-Lindquist-like chart, a linear combination of ∂_t and ∂_ϕ . The angular component is such that $e_0 \pm e_3$ are tangential to the principal null congruences of the metric. Relating between v and t , we choose the following S' observer with

$$e'_0 \sim \frac{\partial}{\partial v} + \frac{r_0 a}{v(r^2 + a^2)} \frac{\partial}{\partial \tilde{\phi}} = \frac{r_0}{v} \left(1 + \frac{r(r^2 + a^2)}{r_0(r^2 - 2\mathcal{M}r + a^2)} \right) \partial_t - \frac{r}{v} \partial_r - \frac{r_0 a}{v(r^2 - 2\mathcal{M}r + a^2)} \partial_\phi + \frac{r_0 a}{v(r^2 + a^2)} \frac{\partial}{\partial \tilde{\phi}}. \quad (64)$$

This choice of e'_0 is also uniquely the one that allows us to write

$$e'_0 \sim e_0 + we_3, \quad (65)$$

for some relative 3-velocity w . Thus the aberration formulas in (62) apply similarly. Recall that in (31), the relevant basis tetrad components read

$$e_0 = e^{-\mu \tilde{T}/M_s} \frac{(r^2 + a^2) \partial_t + a \partial_\phi}{\sqrt{\Sigma \Delta}}, \quad e_3 = -e^{-\mu \tilde{T}/M_s} \sqrt{\frac{\Delta}{\Sigma}} \partial_r, \quad (66)$$

which allows us to read off the 3-velocity as

$$w = \frac{r^2 + a^2}{r^2 + a^2 + \frac{r_0}{r}(r^2 - 2\mathcal{M}r + a^2)}. \quad (67)$$

In the limit of vanishing a , we recover the 3-velocity v for the observer in Vaidya spacetime with $e_0 \sim \frac{\partial}{\partial \tilde{T}}$ as derived in [16]. In the limit $\mu \rightarrow 0$, up to leading order, we have

$$w \approx \mu \left(\frac{r^2 + a^2}{\frac{M_s}{r}(r^2 - 2M_s r + a^2)} \right) + \mathcal{O}(\mu^2). \quad (68)$$

Thus, this reference frame may be relevant for theoretical situations where the observer's velocity is proportional to the strength of the accretion rate, although arguably not so for realistic EHT observations where the accretion is hardly expected to backreact on the metric significantly to affect the 3-velocity of the shadow observer in such a manner.

References

- [1] K. Akiyama *et al.* [Event Horizon Telescope], “First M87 Event Horizon Telescope Results. I. The Shadow of the Supermassive Black Hole,” *Astrophys. J. Lett.* **875**, L1 (2019) doi:10.3847/2041-8213/ab0ec7 [arXiv:1906.11238 [astro-ph.GA]].
- [2] K. Akiyama *et al.* [Event Horizon Telescope], “First Sagittarius A* Event Horizon Telescope Results. I. The Shadow of the Supermassive Black Hole in the Center of the Milky Way,” *Astrophys. J. Lett.* **930**, no.2, L12 (2022) doi:10.3847/2041-8213/ac6674
- [3] H. Falcke, F. Melia and E. Agol, “Viewing the shadow of the black hole at the galactic center,” *Astrophys. J. Lett.* **528**, L13 (2000) doi:10.1086/312423 [arXiv:astro-ph/9912263 [astro-ph]].
- [4] S. E. Gralla, D. E. Holz and R. M. Wald, “Black Hole Shadows, Photon Rings, and Lensing Rings,” *Phys. Rev. D* **100**, no.2, 024018 (2019) doi:10.1103/PhysRevD.100.024018 [arXiv:1906.00873 [astro-ph.HE]].
- [5] J. M. Bardeen, “Timelike and null geodesics in the Kerr metric”, in *Black Holes*, eds. C. DeWitt and B. DeWitt, Gordon and Breach, New York (1973) p. 215
- [6] V. Perlick and O. Y. Tsupko, “Calculating black hole shadows: Review of analytical studies,” *Phys. Rept.* **947**, 1-39 (2022) doi:10.1016/j.physrep.2021.10.004 [arXiv:2105.07101 [gr-qc]].
- [7] K. Akiyama *et al.* [Event Horizon Telescope], “First M87 Event Horizon Telescope Results. V. Physical Origin of the Asymmetric Ring,” *Astrophys. J. Lett.* **875**, no.1, L5 (2019) doi:10.3847/2041-8213/ab0f43 [arXiv:1906.11242 [astro-ph.GA]].
- [8] K. Akiyama *et al.* [Event Horizon Telescope], “First Sagittarius A* Event Horizon Telescope Results. VI. Testing the Black Hole Metric,” *Astrophys. J. Lett.* **930**, no.2, L17 (2022) doi:10.3847/2041-8213/ac6756
- [9] C. Y. Chen, “Testing black hole equatorial reflection symmetry using Sgr A* shadow images,” *Phys. Rev. D* **106**, no.4, 044009 (2022) doi:10.1103/PhysRevD.106.044009 [arXiv:2205.06962 [gr-qc]].
- [10] O. Porth *et al.* [Event Horizon Telescope], “The Event Horizon General Relativistic Magnetohydrodynamic Code Comparison Project,” *Astrophys. J. Suppl.* **243**, no.2, 26 (2019) doi:10.3847/1538-4365/ab29fd [arXiv:1904.04923 [astro-ph.HE]].
- [11] K. Akiyama *et al.* [Event Horizon Telescope], “First Sagittarius A* Event Horizon Telescope Results. V. Testing Astrophysical Models of the Galactic Center Black Hole,” *Astrophys. J. Lett.* **930**, no.2, L16 (2022) doi:10.3847/2041-8213/ac6672
- [12] J. C. McKinney, “General relativistic magnetohydrodynamic simulations of jet formation and large-scale propagation from black hole accretion systems,” *Mon. Not. Roy. Astron. Soc.* **368**, 1561-1582 (2006) doi:10.1111/j.1365-2966.2006.10256.x [arXiv:astro-ph/0603045 [astro-ph]].
- [13] T. Johannsen and D. Psaltis, “Testing the No-Hair Theorem with Observations in the Electromagnetic Spectrum: II. Black-Hole Images,” *Astrophys. J.* **718**, 446-454 (2010) doi:10.1088/0004-637X/718/1/446 [arXiv:1005.1931 [astro-ph.HE]].

- [14] C. k. Chan, D. Psaltis and F. Ozel, “GRay: a Massively Parallel GPU-Based Code for Ray Tracing in Relativistic Spacetimes,” *Astrophys. J.* **777**, 13 (2013) doi:10.1088/0004-637X/777/1/13 [arXiv:1303.5057 [astro-ph.IM]].
- [15] R. Narayan, M. D. Johnson and C. F. Gammie, “The Shadow of a Spherically Accreting Black Hole,” *Astrophys. J. Lett.* **885**, no.2, L33 (2019) doi:10.3847/2041-8213/ab518c [arXiv:1910.02957 [astro-ph.HE]].
- [16] J. Solanki and V. Perlick, “Photon sphere and shadow of a time-dependent black hole described by a Vaidya metric,” *Phys. Rev. D* **105**, no.6, 064056 (2022) doi:10.1103/PhysRevD.105.064056 [arXiv:2201.03274 [gr-qc]].
- [17] P. K. Dahal and D. R. Terno, “Kerr-Vaidya black holes,” *Phys. Rev. D* **102**, 124032 (2020) doi:10.1103/PhysRevD.102.124032 [arXiv:2008.13370 [gr-qc]].
- [18] E. T. Newman and A. I. Janis, “Note on the Kerr spinning particle metric,” *J. Math. Phys.* **6**, 915-917 (1965) doi:10.1063/1.1704350
- [19] A. Grenzebach, V. Perlick and C. Lämmerzahl, “Photon Regions and Shadows of Kerr-Newman-NUT Black Holes with a Cosmological Constant,” *Phys. Rev. D* **89**, no.12, 124004 (2014) doi:10.1103/PhysRevD.89.124004 [arXiv:1403.5234 [gr-qc]].
- [20] J. L. Synge, “The Escape of Photons from Gravitationally Intense Stars,” *Mon. Not. Roy. Astron. Soc.* **131**, no.3, 463-466 (1966) doi:10.1093/mnras/131.3.463
- [21] N. Tsukamoto, “Black hole shadow in an asymptotically-flat, stationary, and axisymmetric spacetime: The Kerr-Newman and rotating regular black holes,” *Phys. Rev. D* **97**, no.6, 064021 (2018) doi:10.1103/PhysRevD.97.064021 [arXiv:1708.07427 [gr-qc]].
- [22] R. Craig Walker, P. E. Hardee, F. B. Davies, C. Ly and W. Junor, “The Structure and Dynamics of the Subparsec Jet in M87 Based on 50 VLBA Observations over 17 Years at 43 GHz,” *Astrophys. J.* **855**, no.2, 128 (2018) doi:10.3847/1538-4357/aaafcc [arXiv:1802.06166 [astro-ph.HE]].
- [23] E. Quataert, “A thermal bremsstrahlung model for the quiescent x-ray emission from sagittarius a*,” *Astrophys. J.* **575**, 855-859 (2002) doi:10.1086/341425 [arXiv:astro-ph/0201395 [astro-ph]].
- [24] F. K. Baganoff, Y. Maeda, M. Morris, M. W. Bautz, W. N. Brandt, W. Cui, J. P. Doty, E. D. Feigelson, G. P. Garmire and S. H. Pravdo, *et al.* “Chandra x-ray spectroscopic imaging of Sgr A* and the central parsec of the Galaxy,” *Astrophys. J.* **591**, 891-915 (2003) doi:10.1086/375145 [arXiv:astro-ph/0102151 [astro-ph]].
- [25] F. Atamurotov, K. Jusufi, M. Jamil, A. Abdujabbarov and M. Azreg-Aïnou, “Axion-plasmon or magnetized plasma effect on an observable shadow and gravitational lensing of a Schwarzschild black hole,” *Phys. Rev. D* **104**, no.6, 064053 (2021) doi:10.1103/PhysRevD.104.064053 [arXiv:2109.08150 [gr-qc]].
- [26] K. Akiyama *et al.* [Event Horizon Telescope], “First M87 Event Horizon Telescope Results. VIII. Magnetic Field Structure near The Event Horizon,” *Astrophys. J. Lett.* **910**, no.1, L13 (2021) doi:10.3847/2041-8213/abe4de [arXiv:2105.01173 [astro-ph.HE]].